Inorganic Chemistry

Article

pubs.acs.org/IC

χ and σ Phases in Binary Rhenium−Transition Metal Systems: a Systematic First-Principles Investigation

Jean-Claude Crivello,* Abedalhasan Breidi, and Jean-Marc Joubert

Chimie Métallurgique des Terres Rares, Institut de Chimie et des Matériaux Paris-Est, CNRS, Université Paris-Est, UMR 7182, 2−8 rue Henri Dunant, 94320 Thiais, France

Supporting Information

ABSTRACT: The Frank−Kasper phases, known as topologically close-packed (tcp) phases, are interesting examples of intermetallic compounds able to accommodate large homogeneity ranges by atom mixing on different sites. Among them, the χ and σ phases present two competing complex crystallographic structures, the stability of which is driven by both geometric and electronic factors. Rhenium (Re) is the element forming the largest number of binary χ and σ phases. Its central position among the transition metals in the periodic table plays an important role in the element ordering in tcp phases. Indeed, it has been shown that Re shows an opposite site preference depending on which elements it is alloyed with. In the present work, χ- and σ-phase stability in binary Re−X systems is systematically studied by a first-principles investigation. The heats of formation of the complete set of ordered configurations (16 for χ and 32 for σ) have been calculated in 16 well-chosen systems to identify stability criteria. They include not only the systems in which χ-Re−X (X = Ti, Mn, Zr, Nb, Mo, Hf, Ta, W) or σ-Re−X (X = V, Cr, Mn, Fe, Nb, Mo, Ta, W) exist but also the systems in which both phases are not stable, including systems in which X is a 3d element from Ti to Ni, a 4d element from Zr to Ru, and a 5d element from Hf to Os. Careful analysis is done of the energetic tendencies as a function of recomposition, size effect, and electron concentration. Moreover, the site preference and other crystallographic properties are discussed. Conclusions are drawn concerning the relative stability of the two phases in comparison with the available experimental knowledge on the systems.

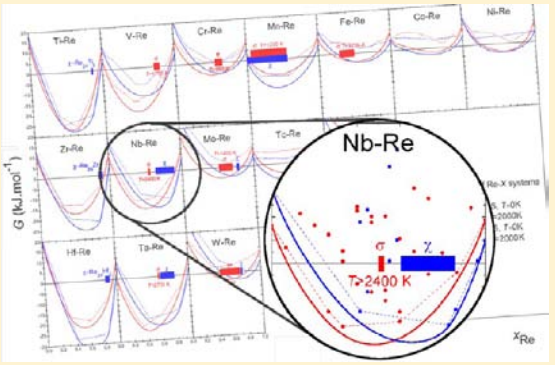

INTRODUCTION

In a multicomponent system, many chemical and physical factors contribute to the stability of one phase over another in competition. Depending on the bonding nature of an alloy, these factors could be the atomic size and electronegativity difference, stabilization by magnetic ordering, etc. Identification of these factors is a real challenge in intermetallic compounds, particulary those accommodating large homogeneity ranges. For instance, the Frank−Kasper phases, also known as topologically close-packed (tcp) phases, exist with large deviation to the stoichiometry and homogeneity ranges accommodated by atom mixing on different sites in a rich variety of systems. Among them, the χ and σ phases present two complex structures with interesting fundamental properties to be analyzed and described. Moreover, these phases hold attractive technological interest. In order to improve the high-temperature mechanical properties, like the creep resistance, of alloys such as steels or nickel-based superalloys, refractory elements (W, Mo, Re, etc.) are added, but they may enhance the detrimental precipitation of intermetallic compounds. Because of the brittle properties of these intermetallics, their precipitation should be avoided.

The field of thermodynamic modeling has been recently stimulated by the progress of techniques allowing the calculation of thermodynamic quantities from first-principle calculations. These methods allow estimation of the formation enthalpies of fully ordered compounds, taking into account their crystal structures. These calculations can be done not only for stable compounds but also for metastable ones, which play an important role in the thermodynamic modeling descriptions. Many recent works have been devoted to the combination of first-principles calculations with modeling techniques such as the Calphad approach.[1−3] Among the tcp phases, the σ phase, in particular its prototype σ-Cr−Fe, has been one of the most studied phases, by many different ab initio methods.[4−8] In addition, many results have already been published on both χ and σ phases in rhenium (Re)-based binary systems Re−X (X = Nb, Mo, Ta, V, W).[9−12] Re is also a constituent of all of the ternary σ phases studied so far by first-principles calculations: σ-Cr−Mo−Re,[13] σ-Cr−Ni−Re,[14] and σ-Mo−Ni−Re.[15] Following their study of the rhodium element,[16] Levy et al. have studied Re[17] as the central element in a high-throughput calculation approach. The number of articles published raises several questions about the interest in this element.

Received: October 2, 2012
Published: March 11, 2013

   dx.doi.org/10.1021/ic302142w | Inorg. Chem. 2013, 52, 3674−3686

Re is interesting for both its fundamental aspects and applications because of its high melting point and resistance to oxidation. In fact, it occupies a central place among the transition metals (TMs) in the periodic table. As can be seen in Figure 1a, Re stands just on the borderline between

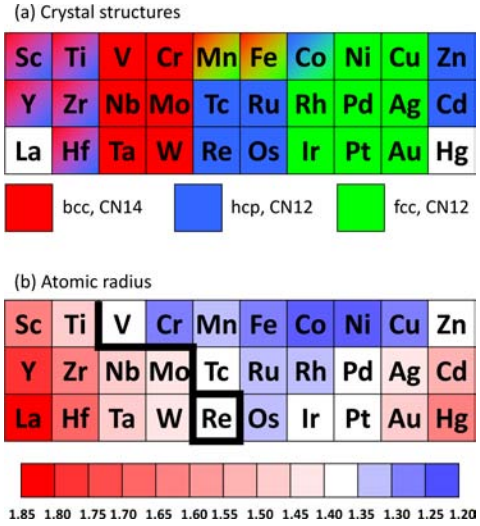

Figure 1. (a) Crystal structures of pure TM elements. (b) Atomic radius (Å) of the element in their solid state. A bold line separates elements larger and smaller than Re.

body-centered-cubic elements and the *d*-electron-richer elements, which crystallize in hexagonal-close-packed (hcp) and face-centered-cubic structures. Like other elements in the middle of the TM series, its cohesive energy is high and, as a consequence, Re presents a small atomic radius in the hcp structure (Figure 1b), whereas elements on its left are larger and elements on its right are smaller in the 4*d* and 5*d* rows. This feature plays an important role on the element ordering in tcp phases, where it has been shown that Re shows an opposite-site preference depending on which elements it is alloyed with. From both theoretical investigations and experimental measurements, a recent study[15] of the ternary σ phase in the Mo−Ni−Re system has shown that Re site preference progressively switches from low coordination number (CN) sites in Mo−Re to high CN in the Ni−Re binary system because of the size effect. Additionally, it is important to mention that Re is the element forming the largest number of known binary χ and σ phases. In this respect, it is a key element to study the binary tcp phase stability.

In the present work, a systematic study of χ- and σ-phase stability in binary Re−*X* systems is done by first-principles investigation. A total of 16 systems have been chosen to identify stability criteria. The selected systems represent a wide and rich variety of X elements including 3*d* from Ti to Ni and 4*d*−5*d* elements in columns 4−10, as indicated in Figure 2. Systems with both stable and metastable phases are included. For both χ and σ phases, all of the ordered configurations have been calculated. Careful analysis is done concerning energetic tendencies as a function of recomposition, electron concentration, size effect, and *d* band filling. The crystallographic properties (equilibrium volume, nonstoichiometry, and site preference) are also discussed.

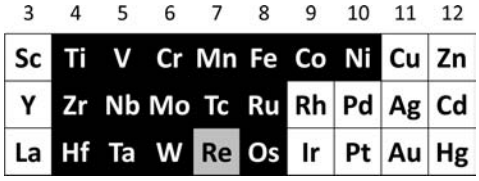

Figure 2. Re−*X* systems investigated in the present paper, where the *X* elements are indicated in black.

GENERAL FEATURES OF THE χ AND σ PHASES

The crystal chemistry of both χ and σ phases has been reviewed in detail by Joubert et al. in refs 18 and 19. Basic and general features are recalled in the following sections.

Crystal Structures. The χ phase is known as α-Mn in the prototype structure (*A*12). It exists in binary compounds with a cubic cell parameter from 8.95 to 12.35 Å.[18] Its space group is $I\bar{4}3m$ with four nonequivalent sites, here called I, II, III, and IV. The four different sites define four different coordination spheres of CN = 16, 16, 13, and 12, respectively. The presence of a coordination polyhedron of CN = 13 is an anomaly, excluding, in principle, this phase from the Frank−Kasper phase group. A representation is given in Figure 3a, and structure parameters are detailed in Table 1. For each *s* site, the f_s ratio indicates the number of first neighbors sharing the same type *s* against the total CN number.

The σ phase ($D8_b$) is tetragonal, described in the $P4_2/mnm$ space group with five nonequivalent positions, here called I, II, III, IV, and V, which present CNs of 12, 15, 14, 12, and 14, respectively (Table 2 and Figure 3b). Owing to the same Wyckoff multiplicity of sites III, IV, and V, eight compositions are degenerated by three configurations each, obtained by atom permutation. Depending on the elements, the lattice parameters extend widely from 8.78 to 10.06 Å for *a* and from 4.55 to 5.23 Å for *c*. The *c*/*a* ratio is observed to be almost constant at approximately 0.52.

Nonstoichiometry and Preferential Site Occupancies. In a binary *A*−*B* system, we define *A* as being the larger element in opposition to *B*, the smaller element. If the χ and σ phases are ordered structures with a complete occupancy of high- and low-CN sites by A and B, respectively, they have the ideal stoichiometries χ-A_5B_{24} or χ-$A_{17}B_{12}$ and σ-A_2B, respectively. However, as stated earlier in the Introduction, tcp phases exist with large homogeneity ranges, even far from their ideal stoichiometries. The accommodation of composition deviation is achieved by *A* and *B* atom mixing on the different *s* sites. However, even if atom mixing occurs to a large extent, complete disorder is never observed because there is always preferential site occupancy. According to our definition, the *A* element presents a preference for sites with large CN and *B* for smaller CN. In 1956, Kasper and Waterstrat[20] proposed that, among elements of the first TM series, those to the right of manganese prefer CN = 12 while those to the left prefer CN = 15 and 16, whereas CN = 14 is proposed to have a mixed occupancy. Moreover, CN = 12 sites have approximate icosahedral symmetry causing high degeneracy of the *d*-like level, as appears in σ-Cr−Ru and -Cr−Os.[21] Therefore, TMs with half-filled *d*-like bands would have high density of states (DOS) when occupying the CN = 12 site, and consequently they should occupy higher-CN sites, which allow a better separation of bonding and antibonding *d* bands.

Among all of the binary Re−*X* systems studied and listed in Figure 2, several *X* elements form χ and/or σ phase(s) upon

dx.doi.org/10.1021/ic302142w | Inorg. Chem. 2013, 52, 3674−3686

Table 1. Crystal Structure of the χ Phase ($A12$): Sites, Wyckoff Positions, Atomic Positions (Average Values) in the Space Group $I\bar{4}3m$ (No. 217)[18] and Details of the First Neighbors, CNs, and f_s Ratios

site s	Wyckoff	x	y	z	I	II	III	IV	CN	f_s
I	2a	0	0	0	0	4	0	12	16	0
II	8c	∼0.317	x	x	1	0	6	9	16	0
III	24g_1	∼0.357	x	∼0.035	0	2	6	5	13	0.46
IV	24g_2	∼0.089	x	∼0.282	1	3	5	3	12	0.25

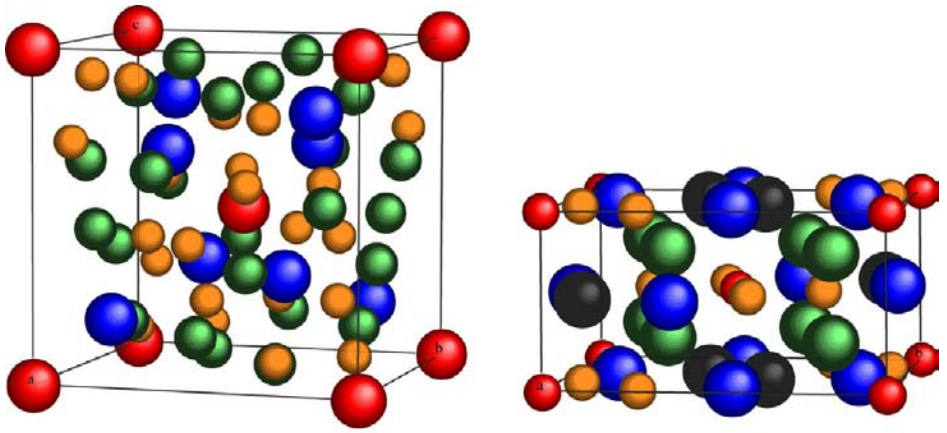

Figure 3. Representative crystal structures of (a) the χ and (b) the σ phases.

Table 2. Crystal Structure of the σ Phase ($D8_b$): Sites, Wyckoff Positions, Atomic Positions (Average Values) in the Space Group $P4_2/mnm$ (No. 136)[19] and Details of the First Neighbors, CNs, and f_s Ratios

site s	Wyckoff	x	y	z	I	II	III	IV	V	CN	f_s
I	2a	0	0	0	0	4	0	4	4	12	0
II	4f	≃0.399	x	0	2	1	2	4	6	15	0.07
III	8i_1	≃0.464	≃0.131	0	0	1	5	4	4	14	0.36
IV	8i_2	≃0.741	≃0.066	0	1	2	4	1	4	12	0.08
V	8j	≃0.187	x	≃0.251	1	3	4	4	2	14	0.14

alloying with Re. These existing systems are χ-Re−X with X = Ti, Mn, Zr, Nb, Mo, Hf, Ta, W and σ-Re−X with X = V, Cr, Mn, Fe, Nb, Mo, Ta, W. Figure 4 indicates whether the χ or σ phase exists and whether X behaves as an A or a B element in the studied systems.

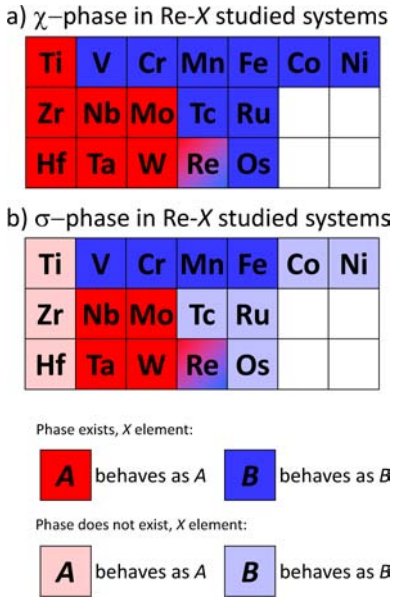

Figure 4. Review of the studied Re−X systems in both χ and σ phases.

MODELS AND METHODOLOGY

The finite-temperature phase equilibrium of the intermetallic compounds can be computed by a combined technique. Using the compound energy formalism (CEF),[22,23] phases are divided into sublattices, with a given number of end members. The heats of formation of all generated ordered configurations are estimated by first-principles calculations. Only the configurational entropy is considered in the calculation of the Gibbs energy as in the Bragg−Williams approximation (BWA),[24] neglecting the short-range-order contributions. A recent review on nonstoichiometry modeling of the Frank−Kasper phases can be found in ref 25.

CEF. In practical thermodynamic applications of materials science, the commonly controlled processing variables are the temperature T, pressure P, and number of atoms of component i N_i, which render the Gibbs energy G as the state function to be modeled and used in the description, like in the Calphad modeling.[26] By neglect of the pressure and volume dependence, the Gibbs energy of a phase φ is linked to the heat of formation H and entropy S by the relation $G^{\varphi} = H^{\varphi} - TS^{\varphi}$.

dx.doi.org/10.1021/ic302142w | Inorg. Chem. 2013, 52, 3674−3686

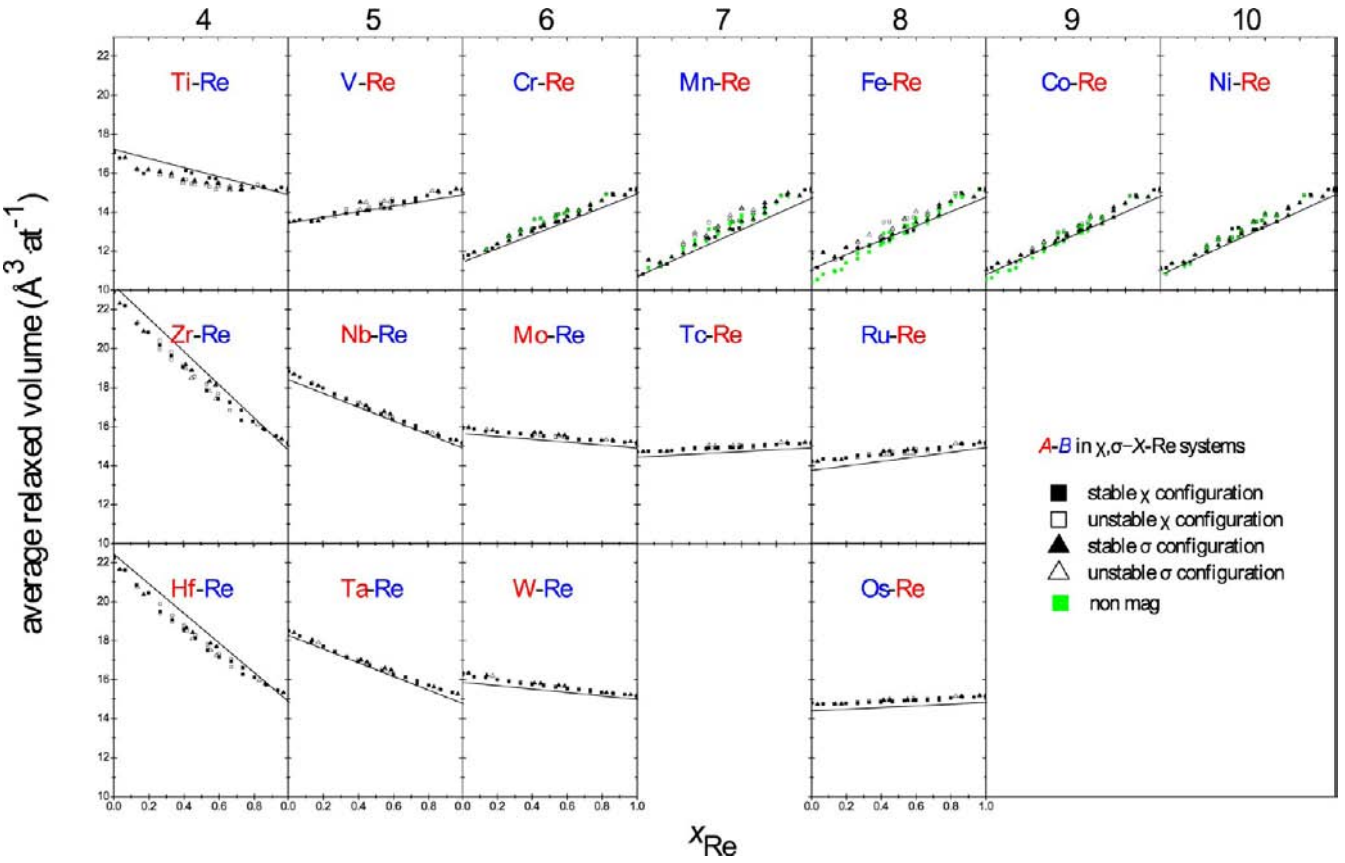

Figure 5. Relaxed volume of each structure in both χ (□) and σ (Δ) phases for the 16 Re−X binary systems. Full symbols represent most stable configurations. For X = Cr, Mn, Fe, Co, Ni, green points represent the volumes from non-spin-polarized calculation. A line joins the volumes of the end compounds in their SER state.

One of the standard ways to describe an intermetallic compound in the Calphad methodology is the description within the CEF. Where x_i is the molar fraction of element i, the Gibbs energy $G^{\varphi}(\{x_i\},T)$ is defined by

$$G^{\varphi}(\{x_i\}, T) = {}^{\mathrm{ref}}G^{\varphi}(\{x_i\}, T) + {}^{\mathrm{id}}G^{\varphi}(\{x_i\}, T) + {}^{\mathrm{ex}}G^{\varphi}(\{x_i\}, T) \quad (1)$$

The Gibbs energy surface of reference, ${}^{\mathrm{ref}}G^{\varphi}(\{x_i\},T)$, represents the site-occupancy-weighted molar enthalpies of the ordered configurations in phase φ, for which no entropy of formation is assumed. In the case of the χ and σ phases of Re−X binaries, it is defined as the following:

$$\begin{cases} {}^{\mathrm{ref}}G^{\chi}(x_{\mathrm{Re}}, x_X, 0) = \sum_{i,j,k,l=\mathrm{Re},X} [y_i^{(\mathrm{I})} y_j^{(\mathrm{II})} y_k^{(\mathrm{III})} y_l^{(\mathrm{IV})}] H_{ijkl}^{\chi,0} \\ {}^{\mathrm{ref}}G^{\sigma}(x_{\mathrm{Re}}, x_X, 0) = \sum_{i,j,k,l,m=\mathrm{Re},X} [y_i^{(\mathrm{I})} y_j^{(\mathrm{II})} y_k^{(\mathrm{III})} y_l^{(\mathrm{IV})} y_m^{(\mathrm{V})}] H_{ijklm}^{\sigma,0} \end{cases} \quad (2)$$

where $y_i^{(s)}$ is the fractional site occupation of species i on the sublattice s, respectively, $H_{ijkl}^{\chi,0}$ and $H_{ijklm}^{\sigma,0}$ are the enthalpies of formation at 0 K of the $\chi - (i, j, k, l)$ and $\sigma - (i, j, k, l, m)$ configurations of compositions x_{Re} and x_{X}, obtained by subtracting the total energy calculated by density functional theory (DFT) and the energies E_i^{SER} of elements in their stable element reference (SER):

$$\begin{cases} H_{ijkl}^{\chi,0} = E_{ijkl}^{\chi} - x_{\mathrm{Re}} E_{\mathrm{Re}}^{\mathrm{hcp}} - x_X E_X^{\mathrm{SER}} \\ H_{ijklm}^{\sigma,0} = E_{ijklm}^{\sigma} - x_{\mathrm{Re}} E_{\mathrm{Re}}^{\mathrm{hcp}} - x_X E_X^{\mathrm{SER}} \end{cases} \quad (3)$$

As an approximation, the tcp phase can be described with ideal mixing on each sublattice, where the configurational entropy is only considered. In other words, the excess Gibbs energy ${}^{\mathrm{ex}}G^{\varphi}(\{x_i\},T)$, due to interactions between atoms sharing the same sublattices, is considered to be null, as in the BWA. This is justified by the fact that, in the χ and σ phase structures, only a few nearest neighbors of a given atom share the same site (see the values of f_s in Tables 1 and 2). Hence, only the configurational entropy is considered to describe the finite temperature properties of the χ and σ phases, as has been shown to be sufficient to reproduce the site occupancies.[10,15,27]

The ideal configurational energy of mixing is the product ${}^{\mathrm{id}}G^{\varphi}(\{x_i\},T) = -T{}^{\mathrm{mix}}S^{\varphi}(\{x_i\})$, where the mixing entropy is given by

$${}^{\mathrm{mix}}S^{\varphi} = -R \sum_s a^{(s)} \sum_{i=\mathrm{Re},X} y_i^{(s)} \ln(y_i^{(s)}) \quad (4)$$

with R the gas constant and $a^{(s)}$ the multiplicity of site s, as given in Tables 1 and 2. For example, expression (4) of the five sublattice model of Re−X in the σ phase is expressed as follows:

dx.doi.org/10.1021/ic302142w | Inorg. Chem. 2013, 52, 3674−3686

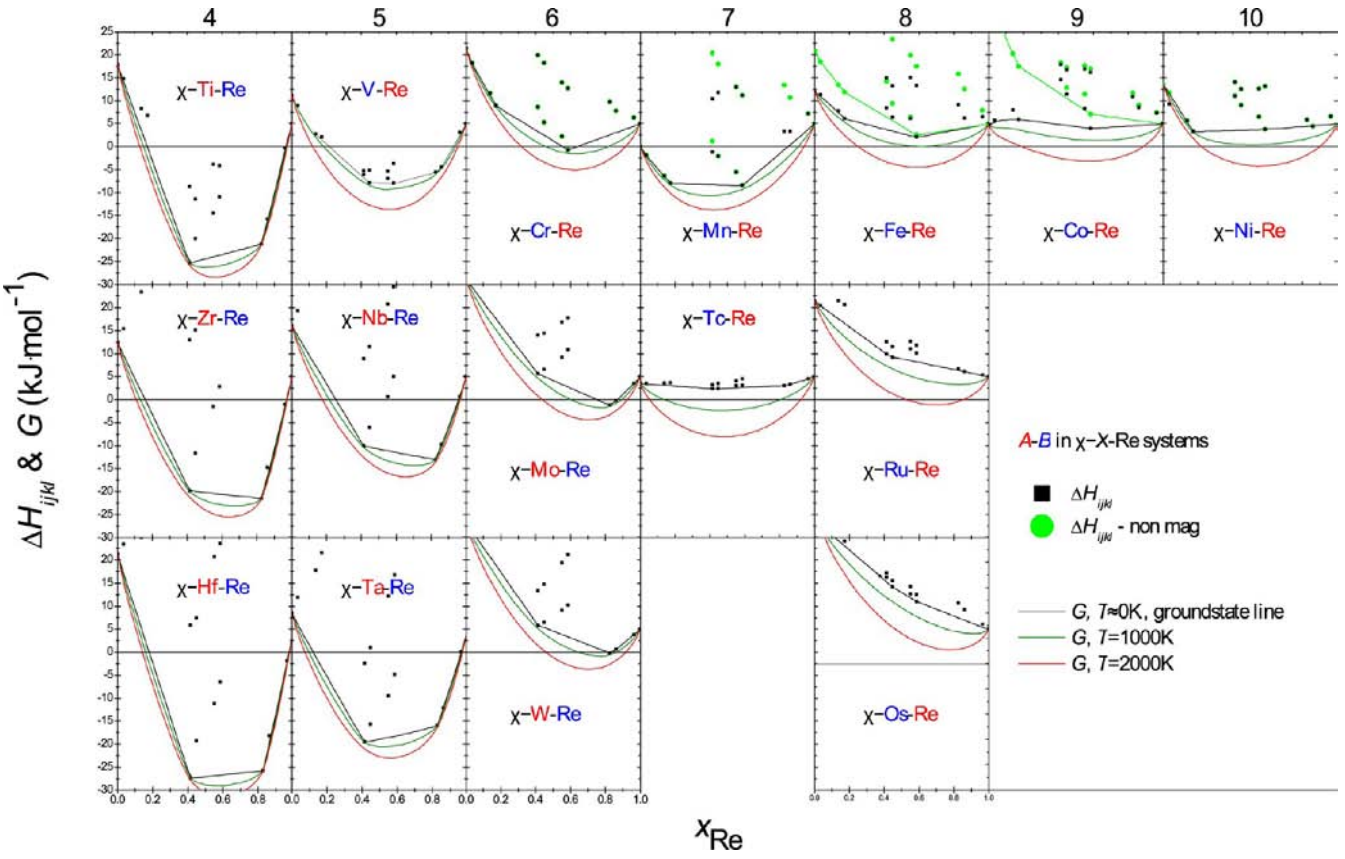

Figure 6. Enthalpies of ordered configurations and Gibbs energies at 1000 and 2000 K of Re−X systems in the χ phase.

$$
\begin{aligned}
{}^{\mathrm{mix}}S^{\sigma} = -R\{2[&y_{\mathrm{Re}}^{(\mathrm{I})}\ln(y_{\mathrm{Re}}^{(\mathrm{I})}) + y_{X}^{(\mathrm{I})}\ln(y_{X}^{(\mathrm{I})})] \\
&+ 4[y_{\mathrm{Re}}^{(\mathrm{II})}\ln(y_{\mathrm{Re}}^{(\mathrm{II})}) + y_{X}^{(\mathrm{II})}\ln(y_{X}^{(\mathrm{II})})] \\
&+ 8[y_{\mathrm{Re}}^{(\mathrm{III})}\ln(y_{\mathrm{Re}}^{(\mathrm{III})}) + y_{X}^{(\mathrm{III})}\ln(y_{X}^{(\mathrm{III})})] \\
&+ 8[y_{\mathrm{Re}}^{(\mathrm{IV})}\ln(y_{\mathrm{Re}}^{(\mathrm{IV})}) + y_{X}^{(\mathrm{IV})}\ln(y_{X}^{(\mathrm{IV})})] \\
&+ 8[y_{\mathrm{Re}}^{(\mathrm{V})}\ln(y_{\mathrm{Re}}^{(\mathrm{V})}) + y_{X}^{(\mathrm{V})}\ln(y_{X}^{(\mathrm{V})})]\} \qquad (5)
\end{aligned}
$$

The calculations consisting of Gibbs energy minimization to find the most stable distribution of the elements on the different sites were performed within *Thermo-Calc* software (version S).[28]

First-Principles Calculation Details. For the 16 chosen binary Re−X systems, all of the end-member compounds in both χ and σ phases have been calculated within the frame of the electronic DFT.[29,30] The distribution of Re and X for every *ijkl* and *ijklm* in χ and σ leads respectively to $2^4 = 16$ and $2^5 = 32$ ordered configurations; i.e., 738 unique tcp compounds have been studied in this paper. For every configuration, DFT calculation has been done in the same conditions and convergence criteria, using the Vienna ab initio simulation package.[31,32] The exchange-correlation potential is described in the generalized gradient approximation with the Perdew−Burke−Ernzerhof functional.[33] An energy cutoff of 400 eV was used for the plane-wave basis. A dense grid sampling of Monkhorst−Pack[34] k mesh was used: 12 × 12 × 12 and 8 × 8 × 15 k points meshing for χ and σ, respectively. Successive optimizations (minimizing internal atomic coordinates and lattice parameters) were done to fully relax each cell structure. The final calculation was performed using the tetrahedron method with Blöchl corrections.[35] The self-consistent total energy calculations converged to less than 0.1 meV. For the binaries Re−X with X = Cr, Mn, Fe, Co, Ni, calculations were done with and without spin polarization. The "Bader" code developed by Henkelman et al.[36,37] has been used to investigate the charge distribution on the atoms, using Bader's topological analysis.[38]

RESULTS

In the Supporting Information (Tables S1 and S2), additional tables provide the complete list of the calculated formation enthalpies (total energies and deducted formation energies) and the crystallographic parameters (cell parameters and internal positions) in the relaxed χ and σ structures, respectively, for the 16 Re−X systems. The total magnetic moment is given for the system calculated as spin-polarized. Each sheet corresponding to a system can be printed in landscape format for a better visual inspection. In addition, the results are given in a TDB file format for free use in thermodynamic modeling purposes.

Relaxed Crystal Structures. Each structure has been fully relaxed to obtain its energy at zero pressure equilibrium. The different crystal parameters (internal atomic coordinates and c/a ratios of the σ tetragonal cell) will not be discussed in detail because they are all centered around the expected average values. However, the volume variation is presented. In Figure 5, the relaxed average atomic volume of each structure in both χ and σ phases is presented for the 16 Re−X binary systems as in a periodic table. Straight lines are guide lines to the eye, indicating a linear variation between volumes of pure elements calculated in their SER structure. One may note the larger volume of pure element calculated in tcp structures, except for

dx.doi.org/10.1021/ic302142w | Inorg. Chem. 2013, 52, 3674−3686

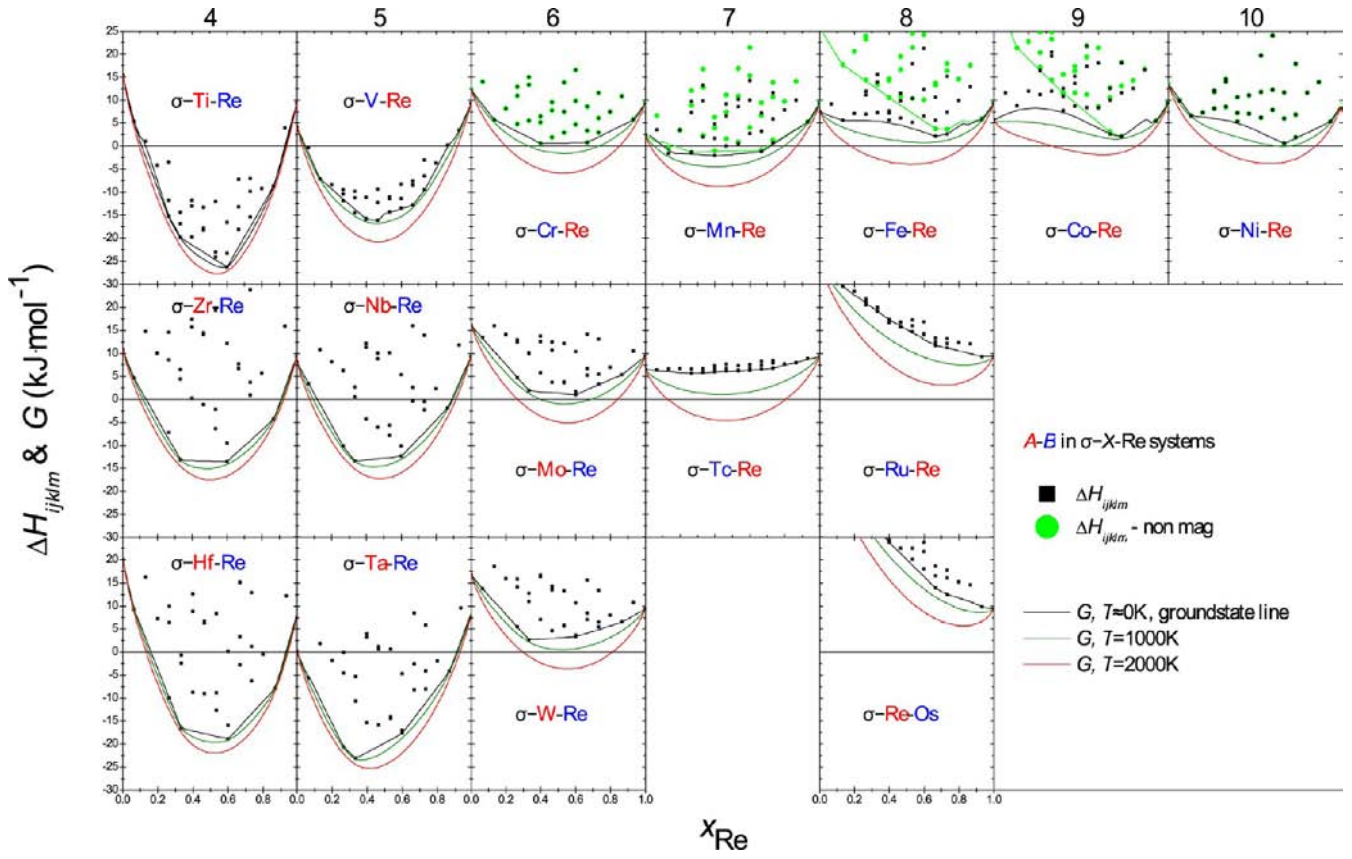

Figure 7. Enthalpies of ordered configurations and Gibbs energies at 1000 and 2000 K of Re−*X* systems in the σ phase.

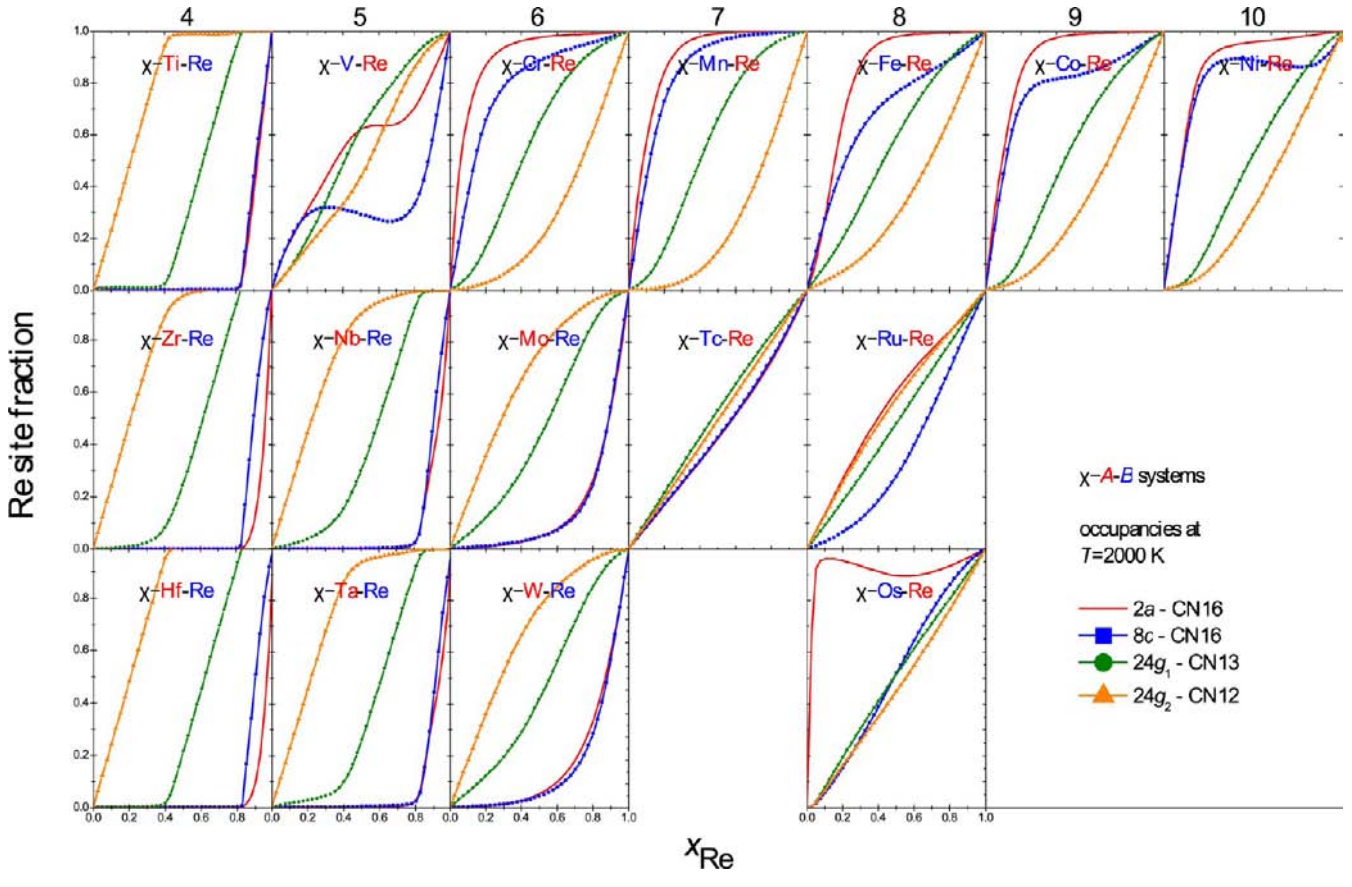

Figure 8. Computed occupancies of Re at 2000 K on the four different sites of the χ phase as a function of the Re composition in the 16 selected binaries.

dx.doi.org/10.1021/ic302142w | Inorg. Chem. 2013, 52, 3674−3686

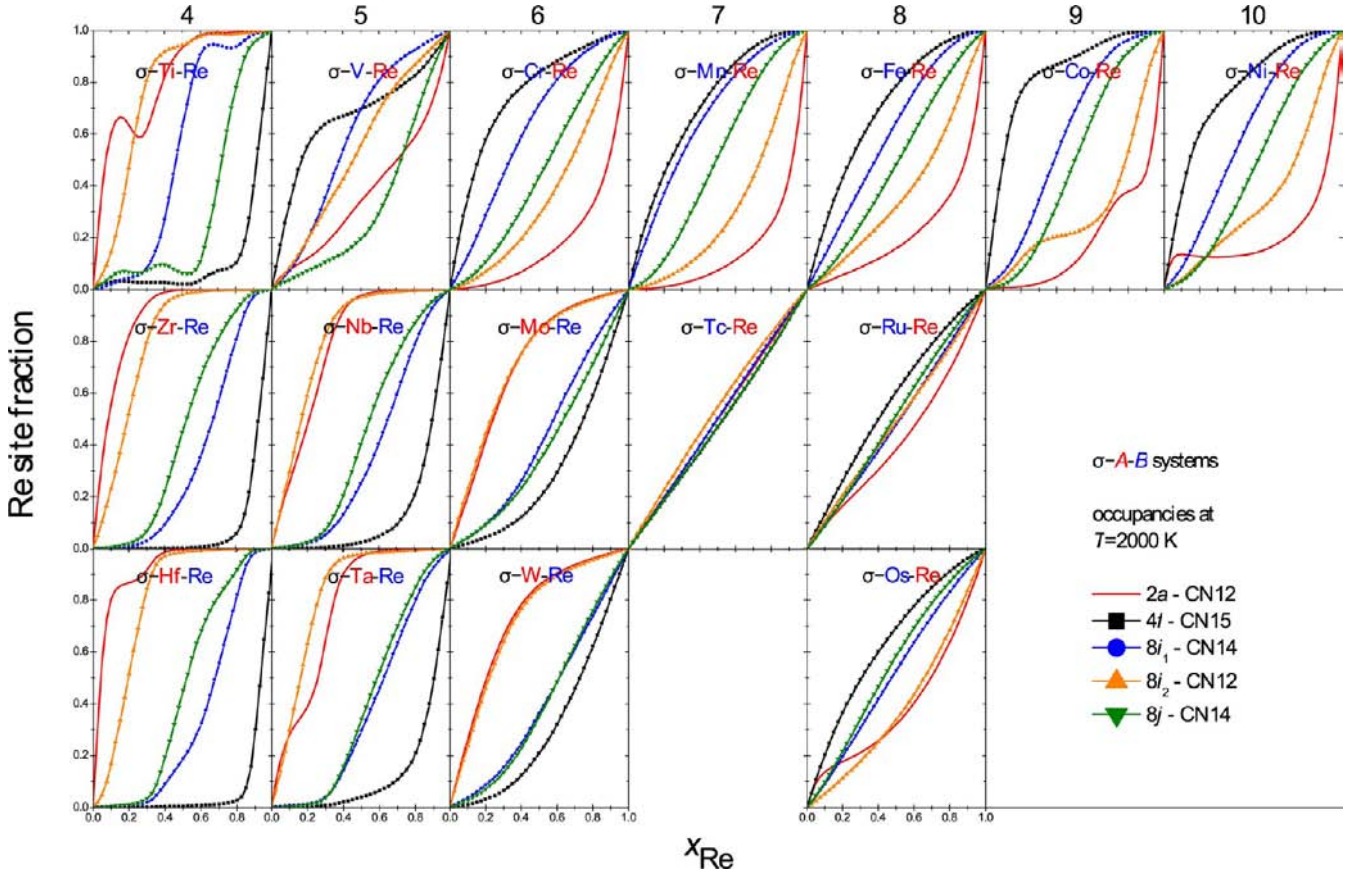

Figure 9. Computed occupancies of Re at 2000 K on the five different sites of the σ phase as a function of the Re composition in the 16 selected binaries.

X = Ti, Zr, Hf. As a function of the Re concentration, the volume decreases or increases, depending on the X element (if the X atom is smaller or larger, respectively). The larger the atomic radius difference is, the larger the variation is. For most systems, the behavior is almost linear and satisfied Vegard's law with respect to the different atomic radii. However, a small deviation to linearity can be seen in systems with X elements in columns 4 and 5, where a denser packing is observed with element mixing.

The χ and σ volumes are similar because the equilibrium volume is dependent on the chemical composition and not on the structure. Several volumes appear at the same composition because of the configuration degeneracy. A comparison of these volumes shows that the smaller cell is generally associated with the most stable configuration; i.e., the denser structures are more stable. For X = Cr, Mn, Fe, Co, Ni, cell volumes that have been spin-polarized are also shown. They are larger than those where spin polarization is not considered, which means that magnetism leads to expansion of the equilibrium volume in the studied tcp phases. This kind of magnetovolume effect has already been observed at the ferromagnetic transition in iron-based intermetallic compounds such as $La(Fe,Si)_{13}$ or $YFe_2D_{4.2}$.[39,40]

Heats of Formation of the Ordered Compounds. The following discussion concerns the heats of formation of ordered compounds at 0 K obtained from DFT calculations and aims to discuss the stability of different configurations by comparing their ΔH^{φ} with their decomposition into pure elements in their DFT-calculated SER state (chosen as the energy origin as a reference). The $\Delta H^{\varphi} < 0$ criteria are not enough to stabilize the φ phase in the phase diagram because the competition with other phases should be considered. On the other hand, a phase with a positive enthalpy of formation may be stabilized at high temperature by the configuration entropy. However, it is an important parameter to assess the stability.

First of all, results on the χ phase are discussed. Figure 6 shows the 16 calculated formation enthalpies ΔH^{χ}_{ijkl} of the 16 Re−X binary systems. Except for the pure manganese, which crystallizes in the $A12$ structure, all pure elements present positive ΔH^{χ}_{iiii} values. The lattice stability of most of the studied elements in $A12$ is large, with more than 10 kJ·mol^{-1} of atoms relative to their SER states. A few systems, namely, i = Ta and Mn isoelectronic elements (Tc and Re), exhibit a rather moderate enthalpy (less than 5 kJ·mol^{-1}). In opposition to pure elements, several binary $ijkl$ configurations present negative ΔH^{χ}_{ijkl} values. This is the case for all binaries with the X element located on the left of Re. Most exothermic ΔH^{χ}_{ijkl} values are obtained with X elements in column 4 ($\sim$−20 kJ·mol^{-1}). For X in column 5, ΔH^{χ}_{ijkl} is about $\sim$−10 kJ·mol^{-1} and is almost 0 for X in column 6. Concerning the binaries with Re isoelectronic elements, Mn−Re presents exothermic ΔH^{χ}_{ijkl} because pure manganese is in its SER state. The binary Tc−Re shows ΔH^{χ}_{ijkl} values independent of the composition and configuration, due to the very similar radii and electronic properties of these two elements. For binaries with X on the right side of Re, all configurations have positive ΔH^{χ}_{ijkl} values, even considering the important magnetic contributions for X = Fe, Co, Ni.

It seems that the formation energy of the χ phase in Re−X increases with the column number of X, while it does not

dx.doi.org/10.1021/ic302142w | Inorg. Chem. 2013, 52, 3674−3686

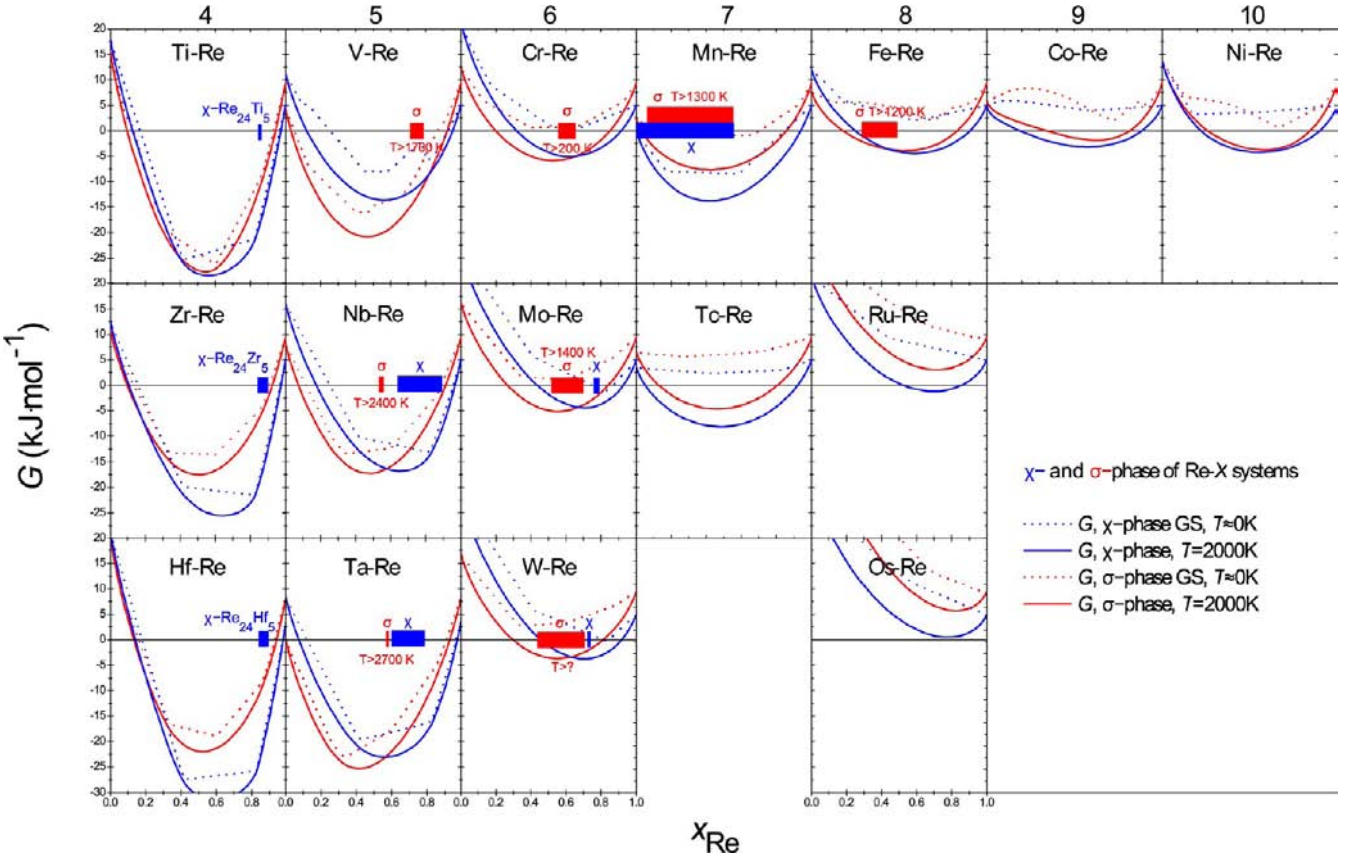

Figure 10. Competition of the phase stability between the χ (blue) and σ phases (red) at 0 and 2000 K (dotted and solid lines, respectively). Blocks located at the energy origin represent the domain of the phases observed experimentally.

depend much on the group period. Thus, the stability of the χ phase should be mainly driven by electronic factors.

Now, the geometric argument is considered. Careful analysis of the *ijkl* configurations shows that when Re is larger than *X*, then the configurations with Re occupying the sites of high CN are more stable, like in the Re*X*Re*XX* and Re*X*Re*X*Re configurations, whereas if Re is smaller than *X*, the configurations with Re on the CN = 12 and 13 sites are more stable.

The results for the σ phase are shown in Figure 7. The lattice stability of pure Re in the σ phase is about 9.3 kJ·mol^{-1}. Only two pure elements, tantalum and manganses, show a tendency to crystallize in the σ-phase structure, having formation enthalpies of 0.11 and 0.15 kJ·mol^{-1}, respectively. The magnetism strongly contributes to reduce ΔH^{σ}_{iiii} for i = Fe and Co (9.0 and 27.7 kJ·mol^{-1}, respectively). Regarding the σ binary configurations, the general trends of stability are quite similar to those of the χ phase. Binaries with *X* to the left of Re are the most exothermic systems, especially for *X* in columns 4 and 5. In fact, all systems with *X* from column 6 and onward present positive $\Delta H^{\sigma}_{ijklm}$ values, with one exception, *X* = Mn. The ground-state line, which is defined as the line joining the most stable configurations obtained by a single atom permutation between the five sites, features convex curves for all systems, except for later 3*d* elements *X* = Fe, Co, Ni. This kind of miscibility gap has already been reported.[14,15]

Similarly to the χ phase case, the geometric argument plays a key role in the distribution of atoms over the sites. If Re is smaller than *X*, it behaves as a B element and shows a preference for CN = 12 sites: configurations Re*XX*Re*X* and Re*XX*ReRe are the most stable ones. A similar argument holds when the Re radius is larger than *X*, which leads to more stable configurations with Re on a high-CN site (as *X*Re*X*Re*X*Re). The radius difference between Re and *X* elements has an additional influence on the scattering of $\Delta H^{\sigma}_{ijklm}$ points. In fact, if the difference is small, like for *X* = V, Tc, Ru, Os, the $\Delta H^{\sigma}_{ijklm}$ values do not span much above the ground state, whereas for a large radius difference, like for *X* = Zr, Hf, Ta, the scattering is important. This property holds for both χ and σ phases.

Finite Temperature Properties. As described above, the finite temperature properties of the tcp phase can be described using the BWA. In addition to the ground-state line, the Gibbs curves computed at 1000 and 2000 K are presented in Figures 6 and 7. The difference between these Gibbs energy curves and the hull corresponds to the configurational Gibbs energy contribution. One may see that it is small in some systems (e.g., Hf−Re), for which a few points define the ground state, while it is large for other system (e.g., Ru−Re), for which many points define the ground state. It may be concluded that, in the latter case, the atom mixing would be much larger. We recall that for a completely disordered system ${}^{id}G^{\varphi}(\{x_i\},T) = -T^{mix}S^{\varphi}(\{x_i\}) = -11.53$ kJ·mol^{-1} for $x_X = 0.5$ at $T = 2000$ K (see eq 4).

The Re computed occupancies at 2000 K on the different sites of both χ and σ phases are shown in Figures 8 and 9, respectively. The well-separated site-filling sequence in the χ phase illustrates a tendency for ordering, except for the binaries with *X* = V, Tc, Ru, Os, as expected. In fact, the four occupancy curves of systems with the latter elements indicate an almost complete disorder. For *X* = Ti, Zr, Hf, Nb, Ta, Mo, W, Re behaves as a *B* element and shows a clear preference for low

dx.doi.org/10.1021/ic302142w | Inorg. Chem. 2013, 52, 3674−3686

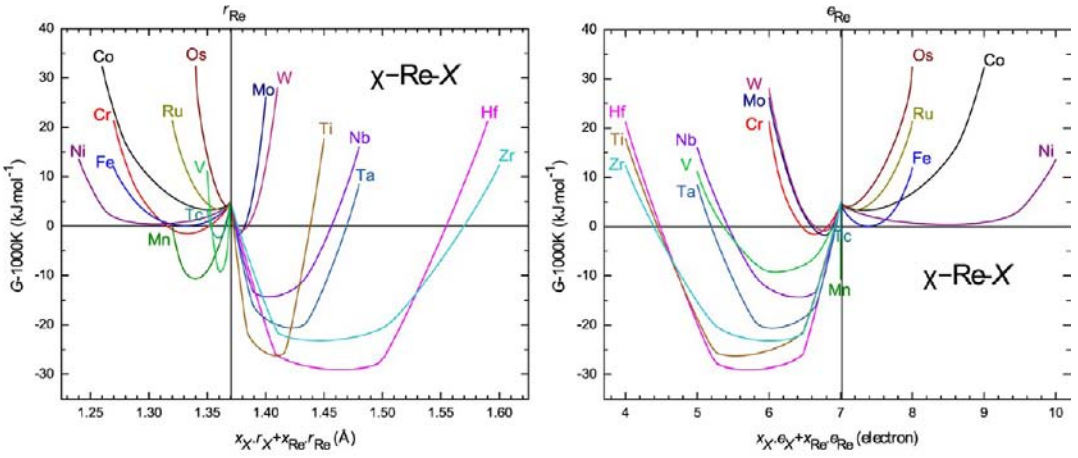

(a) as a function of the average radius (χ phase). (b) as a function of the average valence electron number (χ phase).

(c) as a function of the average radius (σ phase). (d) as a function of the average valence electron number (σ phase).

Figure 11. Computed G at 1000 K,.

CN sites: as Re increases, it first fills the CN = 12 site, then CN = 13, and at last Re replaces X on the two CN = 16 sites simultaneously. Systems with later 3d elements, such as X = Cr, Mn, Fe, Co, Ni, present an inverse Re preference. Now as Re behaves as an A element, an opposite sequence is observed in the site filling from the high- to low-CN sites. The two CN = 16 sites of the χ phase, I and II (2a and 8c), seem to have similar behavior independent of what the system is.

The σ phase site occupancy behavior is comparable to the χ phase one, with respect to the difference that s = 5 sites are now considered, with different multiplicity $a^{(s)}$ and CN as well. The les-ordered systems are Re−Tc, then Re−Ru, Os−Re, and Re−V, and then the Re−X binaries with latter 3d X elements. The most-ordered systems correspond to X elements at the left of Re, X = Ti, Zr, Hf, Nb, Ta, Mo, W, where, in fact, Re behaves as a B element. As for the χ phase, a progressive inversion of Re site preference is observed with the increasing number of valence electrons. If Re behaves as B, it first occupies CN = 12, then CN = 14, and CN = 15 sites, whereas if Re behaves as A, the opposite sequence of progressive filling is observed in all cases: (II) 4f → (III) 8i_1 → (V) 8j → (IV) 8i_2 → (I) 2a. The sites of the same coordination, CN = 12 for I and IV and CN = 14 for III and V, are generally filled simultaneously but behave slightly differently for systems with the 3d X element.

DISCUSSION

Comparison between the χ- and σ-Phase Stability. Analysis of the χ- and σ-phase stability is made without considering the competition with any further phases. The competition of the phase stability between the two phases at 0 and 2000 K is shown in Figure 10. At both temperatures, the three systems of column 4 (Re−Ti, Re−Zr, and Hf−Re) show that the χ phase is more stable than the σ phase in almost the whole composition range. The energy minimum is located around $x_{Re} \simeq 0.6$, not too far from the χ composition (~0.8) that appears in the associated experimental phase diagrams. One may note that the σ phase is absent in these systems, in remarkable agreement with our prediction. Systems with X elements in column 5 show a common stable domain of both phases. Re−V is a kind of exception, probably because of the close atomic radii of the Re and V elements. Re−V supports the stability only for the σ phase, in striking agreement with the experimental phase diagram, where χ does not exist. However, for both Nb−Re and Ta−Re, both phases may coexist with the σ phase in the lower electron concentration domain (poor in Re). A similar behavior is observed when X belongs to column 6. However, the equilibrium between χ and σ at 2000 K is displaced toward Re-richer composition. The σ phase in

dx.doi.org/10.1021/ic302142w | Inorg. Chem. 2013, 52, 3674−3686

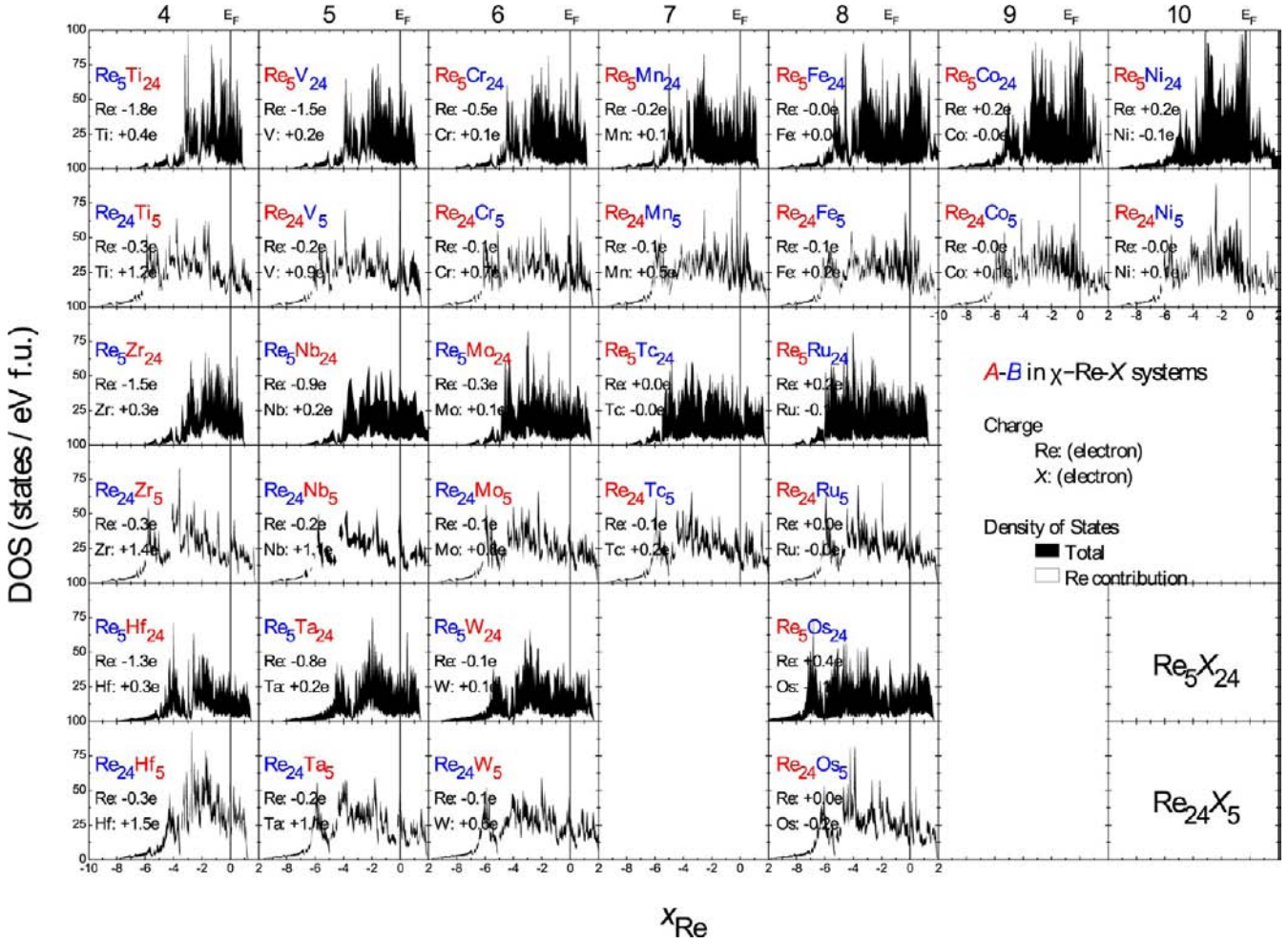

Figure 12. DOSs for the two sets of ordered configurations in the χ phase: Re_5X_{24} and $Re_{24}X_5$ for 16 Re−X systems. White-filled areas correspond to the Re electronic contribution. Bader charge transfers are also indicated.

systems of this column decomposes into pure elements at 0 K, and it is stabilized at high temperature by the configuration entropy. In comparison with available experimental phase diagrams of currently addressed systems, the comparison between the χ- and σ-phase stability presents similar positions regarding the chemical composition but also the temperature (such as σ in X = Cr, Mo, W binaries, which could appear only at high temperature). The case of the isoelectronic elements (X = Mn, Tc) shows that the χ phase is more stable at any composition and temperature. Conclusions for X beyond column 7 are more difficult to draw because energies are positive in the whole range, except at high temperature like in Fe−Re: σ is more stable than χ, in agreement with the experimental composition range. As a conclusion, if the σ phase may appear to be stable, it will be on the lower electron concentration side than the χ phase.

Geometric and Electronic Arguments. As the tcp phase stability is driven by geometric and electronic arguments, computed G curves at 1000 K of both the χ and σ phases are shown for the 16 systems, as a function of the average radius (Figure 11a,c) and as a function of the average valence electron number (Figure 11b,d). Whatever the phase, each graph presents similar features. As far as the average radius is concerned, negative G values are located between 1.30 and 1.57 Å. It is visible that Re forms tcp phases preferentially with larger atoms. Besides, it looks like Re-based χ and σ phases may be formed if there is a contrast of radii, which leads to a better packing of the tcp phase. The same kind of analysis can be made about the average valence electron numbers. Negative G values of Re−X are found between 4.5 and 7 electrons for both phases. These values are not located in the empirical windows observed experimentally for the χ phase (6.2−7.4)[18] but agree as far as the σ phase is concerned (5.5−8).[19] The disagreement illustrates that the negative G values are not a sufficient stability criteria and that competition between all phases has to be taken into account.

To get a clearer picture of the electronic contribution to the phase stability, careful analysis of the electronic structure is made in the following paragraph.

Electronic Structure. Electronic structure analysis is the best method to understand the stability of a phase. Few attempts are done in the following section. Because it is not possible to discuss all of the calculated configurations, two compositions have been selected for both the χ and σ phases. They correspond to the ideal ordering described above, χ-A_5B_{24} and σ-A_2B, respectively, and their antistructure, i.e., all of the {χ-*AABB*, χ-*BBAA*} and {σ-*BAABA*, σ-*ABBAB*} compounds. The electronic DOSs are plotted for the two sets of ordered configurations, χ-{Re_5X_{24};$Re_{24}X_5$} and σ-{ReX_2;Re_2X}, with black-filled areas in Figures 12 and 13. The Fermi level (E_F) is chosen as the origin of energies. The Re contribution is indicated in white-filled areas. For clarity, no angular

dx.doi.org/10.1021/ic302142w | Inorg. Chem. 2013, 52, 3674−3686

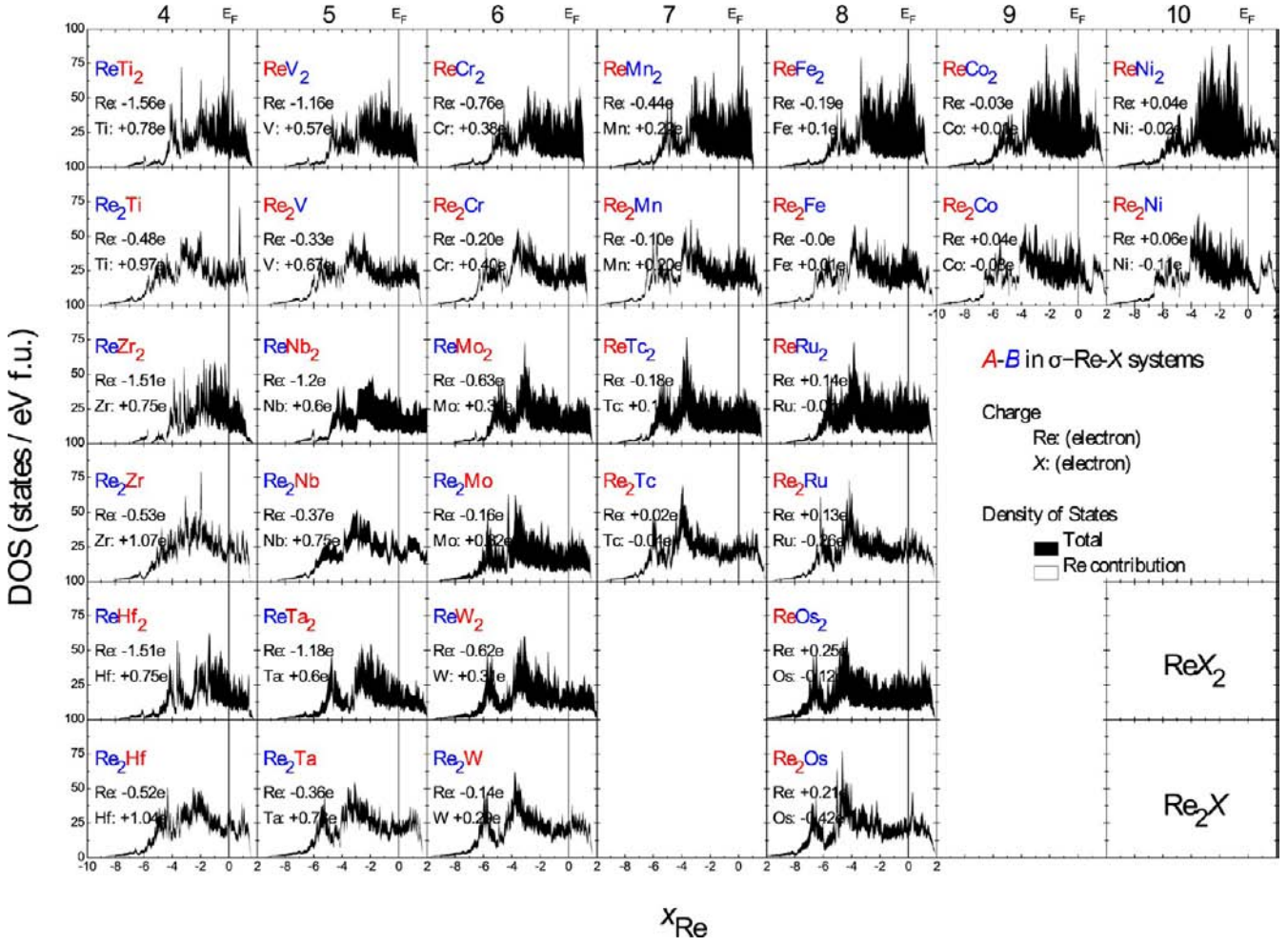

Figure 13. DOSs for the two sets of ordered configurations in the σ phase: ReX_2 and Re_2X for 16 Re−X systems. White-filled areas correspond to the Re electronic contribution. Bader charge transfers are also indicated.

momentum decomposition is shown. For all compounds, the d bands dominate largely the main electronic structure, and no pseudogap at E_F is found, which indicates a metallic bonding behavior.

First, result analysis is done for X in the same column. Whatever the phase, for compounds of the same composition (χ-Re_5Cr_{24}, χ-Re_5Mo_{24}, χ-Re_5W_{24}, σ-Re_2Fe, σ-Re_2Ru, etc.), the electronic structure is found to be very similar, as expected from their isoelectronic character. More interesting is a comparison of the DOSs of a structure and its antistructure in the same system. For example, electronic structures of χ-Re_5Ti_{24} and χ-$Re_{24}Ti_5$ are different because of their chemical composition but also because of their structural arrangement. In this system, Re, which is smaller, behaves as a B element and has a preference for lower-CN sites. As a consequence, the DOS of χ-$Re_{24}Ti_5$ is indicative of a larger electronic stability than that of χ-Re_5Ti_{24} because (i) the main structure is less localized and extends toward lower energies and (ii) the Fermi level falls in a valley region of DOS. The same arguments could be used if Re behaves as an A element, as in χ-Re−Os: χ-Re_5Os_{24} presents a large main structure, with lower DOS at E_F. One may note that some expected stable compounds present unstable electronic features: for example, E_F of χ-$Re_{24}W_5$ is located in a peak of DOS. However, it could be stabilized by a slight composition change capable of shifting the Fermi level to a valley of DOS. This is what is observed for this compound stabilized in the phase diagram at a W-richer composition. In the case of the σ phase, A_2B compounds are expected to present a more stable electronic structure than AB_2 compounds. It appears that if Re behaves as A, like in the Re−V system, σ-Re_2V presents a broader structure with a low value of DOS at E_F, whereas σ-ReV_2 has a dense main structure. On the other hand, in the Re−W system, where Re behaves as B, the σ-ReW_2 main structure is pretty broad but not as large as σ-Re_2W because of its richer Re concentration and thus presents a low DOS value at E_F.

Second, analysis is done as a function of the X column number. As expected from the rigid-band model, a progressive d-band filling is observed for compounds with X elements from left to right in the same series. The center of the Re d bands (see the Re contribution in white-filled areas in Figures 12 and 13) is found to be shifted to higher energy as the X atomic number increases. Actually, careful analysis of the Bader charge shows that electronic transfer from X to Re decreases from column 4 to 7: if X is located at the left of Re, then Re gains electrons, whereas if X is located at its right, Re transfers electrons to X. This result is found whatever the phase is.

Only paramagnetic states are presented in the present DOS figures. Especially, if X = Fe and Co, the DOS at E_F is pretty high even for the expected stable composition. This effect leads to a greater tendency to magnetism via the usual Stoner feedback. It can be shown in Figures 6 and 7 how much the

dx.doi.org/10.1021/ic302142w | Inorg. Chem. 2013, 52, 3674−3686

enthalpies are more stable in ferromagnetic states. An electronic structure analysis of the ferromagnetism will be done in a future paper.[41]

CONCLUSIONS

For 16 Re−X binary systems, a complete set of ordered configurations (16 for χ and 32 for σ) has been calculated by first principles. A systematic analysis was done of the energetic tendencies as a function of the Re composition, electron concentration, and size effect. Moreover, the site preference and other crystallographic properties have been discussed. From this systematic investigation, two major stability trends can be drawn: (i) the geometric criterion governs the choice of ground-state configurations and (ii) the electronic criterion governs the magnitude of the exothermicity. If X belongs to column 5 or 6, in spite of having the same electron number, most stable configurations depend on whether X is a 3d element (smaller atom) or other 4d or 5d element (larger atoms). For the former criterion, the size effect controls which configurations are the most stable with respect to larger atoms, which are favorable on high-CN sites and smaller on low-CN sites. Site-filling sequences respect the same geometric preferences with an important ordering if the radius difference is important; on the other hand, the structure looks more disordered if the radii are too close. Additionally, the electronic criterion does not control the choice of ground-state configurations; however, it will affect the exothermicity (amplitude of the $\Delta H^{0,\varphi}$ value). Negative $\Delta H^{0,\varphi}$ values are obtained between 4.5 and 7 electrons, thus with X located at left of Re. For X chosen from left to right of the same row (with a valence electron increase), a progressive increase of $\Delta H^{0,\varphi}$ is observed for both phases. If both phases are stable, the σ phase appears at lower electron concentration (right of χ). Regarding the chemical composition and the temperature, the comparison between the χ- and σ-phase positions presents good correlation with the experimental phase diagrams.

ASSOCIATED CONTENT

Supporting Information

Complete list of the calculated formation enthalpies (total energies and deducted formation energies) and the crystallographic parameters (cell parameters and internal positions) in the relaxed χ and σ structures, respectively, for the 16 Re−X systems (Tables S1 and S2). This material is available free of charge via the Internet at http://pubs.acs.org.

AUTHOR INFORMATION

Corresponding Author

*E-mail: crivello@icmpe.cnrs.fr.

Notes

The authors declare no competing financial interest.

ACKNOWLEDGMENTS

Financial support from the Agence Nationale de la Recherche (Project Armide 2010 BLAN 912 01) is acknowledged. This work was performed using HPC resources from GENCI-CINES/IDRIS (Grant 2012-096175). The contribution of Pierre Joubert to the proof reading of the manuscript is greatly appreciated. Nathalie Dupin is acknowledged for useful discussions and comments.

REFERENCES

(1) Burton, B. P.; Dupin, N.; Fries, S. G.; Grimvall, G.; Fernandez-Guillermet, A.; Miodownik, P.; Vinograd, W. A. O. V. *Z. Metallkd.* **2001**, *92*, 514−525.
(2) Kaufman, L.; Turchi, P. E. A.; Huang, W.; Liu, Z. *CALPHAD* **2001**, *25*, 419−433.
(3) Wolverton, C.; Yan, X.-Y.; Vijayaraghavan, R.; Ozoliņš, V. *Acta Mater.* **2002**, *50*, 2187−2197.
(4) Sluiter, M. H. F.; Esfarjani, K.; Kawazoe, Y. *Phys. Rev. Lett.* **1995**, *75*, 3142−3145.
(5) Korzhavyi, P.; Sundman, B.; Selleby, M.; Johansson, B. *Mater. Res. Soc. Symp. Proc.* **2005**, *842*, S4.10.1.
(6) Pavlů, J.; Vřeštál, J.; Šob, M. *Intermetallics* **2010**, *18*, 212−220.
(7) Cieslak, J.; Tobola, J.; Dubiel, S. M.; Sikora, W. *Phys. Rev. B* **2010**, *82*, 224407.
(8) Kabliman, E.; Blaha, P.; Schwarz, K.; Ruban, A. V.; Johansson, B. *Phys. Rev. B* **2011**, *83*, 092201.
(9) Hammerschmidt, T.; Seiser, S.; Drautz, R.; Pettifor, D. Superalloys 2008. *Proceedings of the TMS International Conference*, New Orleans, LA, 2008; The Minerals, Metals and Materials Society: Warrendale, PA, 2008; pp 847−853.
(10) Crivello, J.-C.; Joubert, J.-M. *J. Phys.: Condens. Matter* **2010**, *22*, 035402.
(11) Seiser, B.; Hammerschmidt, T.; Kolmogorov, A. N.; Drautz, R.; Pettifor, D. G. *Phys. Rev. B* **2011**, *83*, 224116.
(12) Palumbo, M.; Fries, S. G.; Hammerschmidt, T.; Drautz, R.; Abe, T.; Crivello, J.-C.; Breidi, A.; Joubert, J.-M. 2013, Submitted for publication.
(13) Crivello, J.-C.; Palumbo, M.; Abe, T.; Joubert, J.-M. *CALPHAD* **2010**, *34*, 487−494.
(14) Palumbo, M.; Abe, T.; Fries, S. G.; Pasturel, A. *Phys. Rev. B* **2011**, *83*, 144109.
(15) Yaqoob, K.; Crivello, J.-C.; Joubert, J.-M. *Inorg. Chem.* **2012**, *51*, 3071−3078.
(16) Levy, O.; Chepulskii, R. V.; Hart, G. L. W.; Curtarolo, S. *J. Am. Chem. Soc.* **2010**, *132*, 833−837.
(17) Levy, O.; Jahnátek, M.; Chepulskii, R. V.; Hart, G. L. W.; Curtarolo, S. *J. Am. Chem. Soc.* **2011**, *133*, 158−163.
(18) Joubert, J.-M.; Phejar, M. *Prog. Mater. Sci.* **2009**, *54*, 945−1058.
(19) Joubert, J.-M. *Prog. Mater. Sci.* **2008**, *53*, 528−583.
(20) Kasper, J. S.; Waterstrat, R. M. *Acta Crystallogr.* **1956**, *9*, 289−295.
(21) Sluiter, M. H. F.; Pasturel, A. *Phys. Rev. B* **2009**, *80*, 134122.
(22) Sundman, B.; Ågren, B. J. *J. Phys. Chem. Solids* **1981**, *42*, 297−301.
(23) Ansara, I.; Burton, B.; Chen, Q.; Hillert, M.; Fernandez-Guillermet, A.; Fries, S. G.; Lukas, H. L.; Seifert, H.-J.; Oates, W. A. *CALPHAD* **2000**, *24*, 19−40.
(24) Bragg, W. L.; Williams, E. J. *Proc. R. Soc. London, Ser. A* **1934**, *145*, 699−730.
(25) Joubert, J.-M.; Crivello, J.-C. *Appl. Sci.* **2012**, *2*, 669−681.
(26) Sundman, B.; Lukas, H. L.; Fries, S. G. *Computational Thermodynamics: The Calphad Method*; Cambridge University Press: Cambridge, U.K., 2007.
(27) Fries, S. G.; Sundman, B. *Phys. Rev. B* **2002**, *66*, 012203.
(28) Sundman, B.; Jansson, B.; Andersson, J.-O. *CALPHAD* **1985**, *9*, 153−190.
(29) Kohn, W.; Sham, L. *Phys. Rev.* **1965**, *140*, A1133−1140.
(30) Sham, L.; Kohn, W. *Phys. Rev.* **1966**, *145*, 561−567.
(31) Kresse, G.; Furthmüller, J. *Phys. Rev. B* **1996**, *54*, 11169−11186.
(32) Kresse, G.; Joubert, D. *Phys. Rev. B* **1999**, *59*, 1758.
(33) Perdew, J. P.; Burke, K.; Ernzerhof, M. *Phys. Rev. Lett.* **1997**, *78*, 1396.
(34) Monkhorst, H.; Pack, J. *Phys. Rev. B* **1976**, *13*, 5188−5192.
(35) Blöchl, P. E.; Jepsen, O.; Andersen, O. K. *Phys. Rev. B* **1994**, *49*, 16223.
(36) Henkelman, G.; Arnaldsson, A.; Jónsson, H. *Comput. Mater. Sci.* **2006**, *36*, 354−360.

(37) Bader charge analysis, http://theory.cm.utexas.edu/vtsttools/bader/.
(38) Bader, R. F. W. In *Atoms in Molecules. A Quantum Theory*; York, N., Ed.; Oxford University Press: Oxford, U.K., 1990.
(39) Fujita, A.; Fujieda, S.; Fukamichi, K.; Mitamura, H.; Goto, T. *Phys. Rev. B* **2001**, *65*, 014410.
(40) Paul-Boncour, V.; Guillot, M.; André, G.; Bourée, F.; Wiesinger, G.; Percheron-Guégan, A. *J. Alloys Compd.* **2005**, *404*−*406*, 355−359.
(41) Breidi, A.; Crivello, J.-C.; Joubert, J.-M. In preparation.